中國機械工程學刊第三十七卷第五期第497~507 頁(民國一百零五年)
Journal of the Chinese Society of Mechanical Engineers, Vol.37, No.5, pp497~507 (2016)

Design and Analysis of Axial Flux Permanent Magnet Motor with Variable Windings

Jyh-Cheng Yu, Ming-Te Cheng, and Wu-Sung Yao*

Department of Mechanical and Automation Engineering
National Kaohsiung First University of Science and Technology
No. 1 University Rd., Yanchao District, Kaohsiung City 824, TAIWAN.
* Corresponding Author: wsyao@nkfust.edu.tw

Keywords: Axial flux permanent-magnet motor, wye winding, delta winding, serial-wye

ABSTRACT

Direct drive hub motors drive a wheel directly without a transmission by incorporating the motor into the hub of wheel, which greatly simplifies the mechanical structure and improves driving performance. This paper presents an alternative approach to design axial flux permanent-magnet (AFPM) motor with winding switch for in-wheel drive vehicle applications. Emphasis is placed on theoretical modeling of AFPM motors with variable winding configuration. For electric vehicle application, a dual-wye winding configuration is proposed, which includes a variable windings between serial-wye and spaced-wye windings. The serial-wye winding is used for motor operation at low speed to generate high torque; while reaching a steady state, the motor is switched to a spaced-wye winding to increase speed. For the variable windings switch, a soft switch method is introduced to smoothly reduce the magnetic flux coupling and prevent jerking and jolting at the windings switching point. A prototype AFPM motor with rated 476W output power at 125 rad/s was constructed to validate the results obtained from the proposed analytical model. Also, the experimental results show that, by switching the serial-wye to wye windings, the magnetic field is reduced by 50% and the motor speed increases by 44% under a load of 5 Nm.

INTRODUCTION

Axial flux permanent-magnet (AFPM) motors have long been developed for electric vehicle applications. In general, the magnetic flux generated from the interaction between the stator coils and the permanent magnet (PM) on the rotor plates can be either in axial or radial directions. Advantages of AFPM motors over conventional radial flux permanent-magnet (RFPM) motors include high torque/weight ratio, superior efficiency, adjustable gap, balanced rotor-stator attractive forces, and better heat-removal. Therefore, AFPM motors can be easily and compactly mounted onto an electric vehicle wheel, and suitable for direct drive applications[1][2]. However, compared to RFPM motors, AFPM motors have unique construction for different applications, which includes a complex magnetic circuit design requiring three-dimensional (3D) finite element analysis (FEA). To design AFPM motor has to consider the tradeoff between simulation time and computational accuracy. Analytical model and two-dimensional (2D) FEA can only provide approximate guidelines for the motor dimensions due to the inherent 3D characteristics of AFPM motors. However, the accuracy of 3D FEA will be at the cost of computation time.

Previously, applications of AFPM motors are limited due to insufficient magnetic energies to fully elaborate their features. Recent breakthroughs in magnetic material technologies and the development of rare earth magnets have helped AFPM motors to improve potential performance and industrial applications. AFPM motors are therefore popularly adopted in recent applications of hard drives, robot joints, fans, compact electric vehicles, wind power generation, aerial vehicle propellers, and other devices that are space-limited. Figures 1 shows the structures of RFPM (Fig. 1(a)) and AFPM (Fig. 1(b)) motors. In general, AFPM motors can be designed as double or single sided, with or without armature slots, with internal or external rotors, and with surface mounted or interior type permanent magnets. Low power AFPM motors usually adopt slotless windings and surface mounted PM. Motor rotors can be embedded into power transmission components to simplify mechanical structures and improves driving efficiency. It can be noted that the rotor and the iron core of RFPM motors have low usage rates. In long stack height designs, heat generated from the coils cannot be easily dissipated, which increases coil resistance and drastically reduces motor efficiencies. AFPM motors yield comparatively high diameter-stack height ratios and high power densities in applications where reduced iron core materials are preferred.

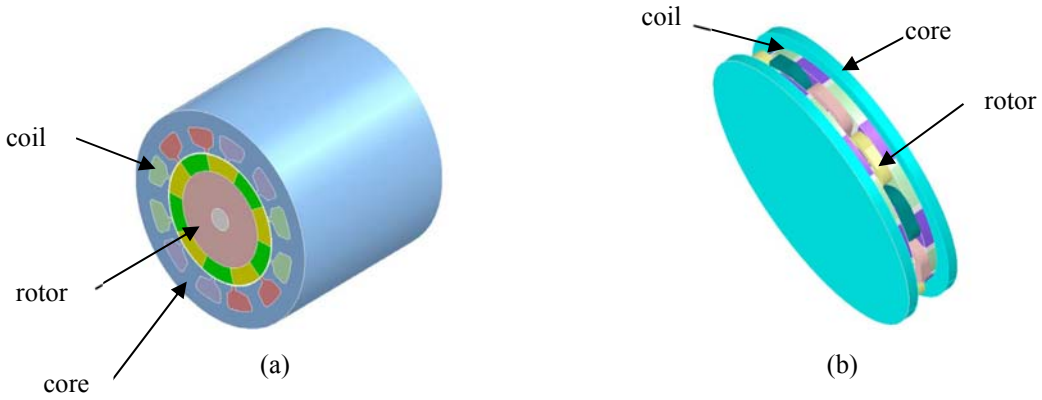

Fig. 1 Schematic representations of (a) RFPM motors and (b) AFPM motors

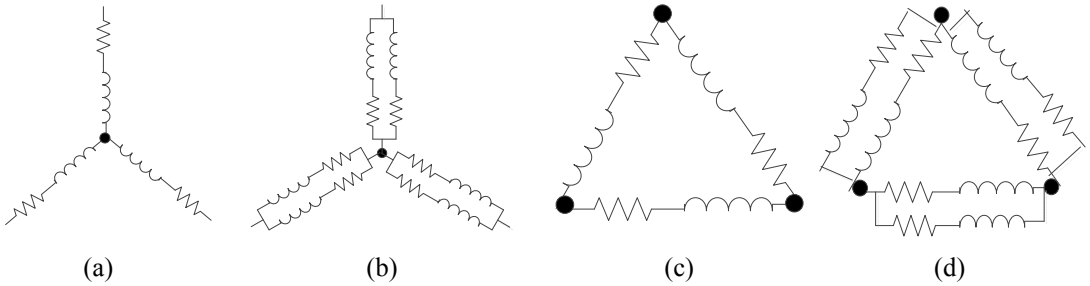

Fig. 2 Various winding connections: (a) wye, (b) double-wye, (c) delta, and (d) double-delta.

To achieve high performance of AFPM motor, the designs of permanent-magnet skewing, winding, and structure dimensions should be considered. Also, increased pole number of AFPM motors can reduce the flux length to improve the torque density [3][4][5]. In general, a wider speed operating range is desirable in the driving applications of electric vehicle. The maximum speed of AFPM machines is limited by the available voltage with a required electromotive force (EMF). Higher speed operation can be achieved by using an inverter with a larger voltage rating or by selecting a motor with lower EMF. Motors with lower EMF have a higher amp/torque ratio characteristic, which results in a bulkier and more expensive inverter. For AFPM motor applied to electric vehicles, a magnetic field weakening technique [6][7] is often used to obtain a higher speed without increasing the driving power. However, it is difficult to reduce the magnetic field of a PM motor because the inductance in the magnetization direction tends to be low.

Nowadays, switched stator windings are often utilized to achieve the efficacy of field weakening. General winding connections of brushless PM motor include wye, double-wye in parallel, delta, and double-delta windings, which are shown in Fig. 2 The related torques for each winding connections from measured back EMF wave forms can be obtained as *wye:delta:double-wye:double-delta* = 1:0.58:0.52:0.29. Theoretically, switching among connections is equivalent to shifting a transmission with variable gear ratios. Vansompel et al. [8] proposed a combined wye-delta connection for switched stator windings to improve motor speed. Pleiss [9] adopted a switching double-delta winding, and Auinger [10] suggested a switching double-wye in parallel winding to improve the torque output in RFPM and AFPM motors.

To reach a wider operation speed range in electric vehicle applications, a combined wye-delta connection winding can often be found in AFPM motors. As shown in Fig. 2, switching of serial and parallel is possible if the phase windings can be divided into several parts. Combinations of serial and parallel coils usually offer a sufficient motor speed. A typical combined wye-delta connection comprises six power switches of S1~S6 as shown in Fig. 3. The winding is wye-connected when switches S1, S2, and S3 are on and the rest are off, and turns to a delta connection by turning S4, S5, and S6 on and the rest off.

Observing Fig. 3, the electric impedance of the wye connection is three times that of delta connection. The back EMF constant and the torque constant of wye connection are 1.732 times those of delta connection, while the rated motor speed of delta connection is 1.732 times that of wye connection. Therefore, the wye connection is applied in initial acceleration and uphill climbing to provide high output torque, the wye connection is applicable when the vehicle reaches a steady state to increase motor speeds. Through torque-speed coordination, a combined wye-delta connection can analogized to a two-stage transmission as shown in Fig. 4.

The maximum speed is limited by the available voltage for a given counter electromotive force value in PM motors. The extension of speed range can be achieved by using the field weakening principle, resulting in constant-power characteristics, but is limited by machine parameters and inverter rating. The combined wye-delta method remains popular for extending the constant-power range without sacrificing the torque capability at higher speeds. Conventionally, the combined wye-delta method employs mechanical contactors that have limited life and are associated with dead time in the range of tens to

hundreds of milliseconds due to mechanical constraints. Power-electronic versions of the contactors have been proposed, but they are rather complicated and involve many switching devices. Although a combined wye-delta electronic shift is feasible, the method tends to generate sparks during switching, which causes a safety concern and requires additional costs for safety circuit installations [11]. This paper proposes a dual-wye winding consisting of a soft switch between a serial-wye and spaced-wye connections, as shown in Fig. 5, which provides high output torque and wide speed range for driving requirements. A theoretical modeling and the experimental results of the AFPM motor with dual-wye windings are presented and compared with those of combined wye-delta connections to demonstrate the feasibility and advantage of the proposed design.

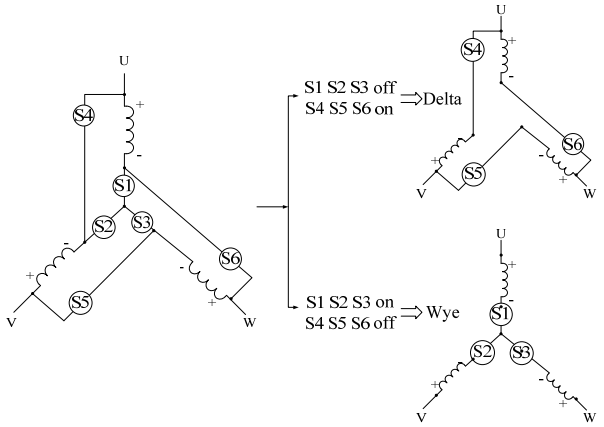

Fig. 3 Winding diagrams of combined wye-delta connection

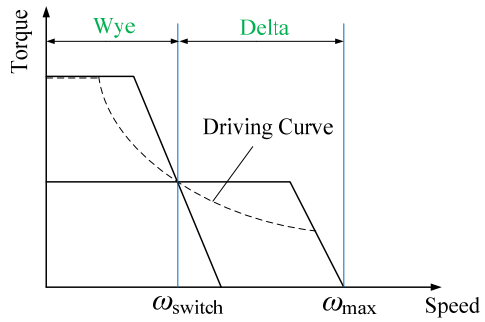

Fig. 4 Speed, torque, and vehicle driving curves with combined wye-delta connections

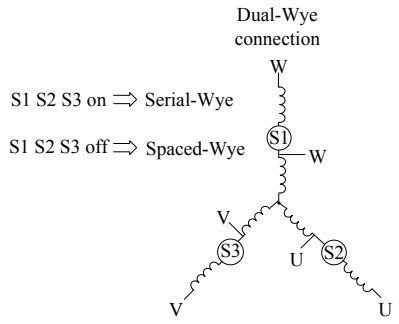

Fig. 5 Dual-wye winding consisting of a serial-wye and spaced-wye connections

MODELING OF AFPM MOTORS WITH VARIABLE WINDINGS

(1) Dynamic model of motor with delta winding connection

The system dynamics of an AFPM motor with three-phase delta winding as shown in Fig. 6 is derived using Kirchhoff's current and voltage laws as follows. The following equations can be obtained.

$$\begin{bmatrix} V_{as}-V_{bs} \\ V_{bs}-V_{cs} \\ V_{cs}-V_{as} \end{bmatrix} = \begin{bmatrix} R_a & 0 & 0 \\ 0 & R_b & 0 \\ 0 & 0 & R_c \end{bmatrix} \begin{bmatrix} I_{as} \\ I_{bs} \\ I_{cs} \end{bmatrix} + \frac{d}{dt} \begin{bmatrix} L_a & L_{ab} & L_{ac} \\ L_{ba} & L_b & L_{bc} \\ L_{ca} & L_{cb} & L_c \end{bmatrix} \begin{bmatrix} I_{as} \\ I_{bs} \\ I_{cs} \end{bmatrix} + \begin{bmatrix} E_a \\ E_b \\ E_c \end{bmatrix} \quad (1)$$

where V_{as}, V_{bs}, and V_{cs} are the stator voltages;
I_{as}, I_{bs}, and I_{cs} are the stator currents;
L_a, L_b, and L_c are the self-inductances;
E_a, E_b, and E_c are the back electromotive forces, and R_a, R_b, and R_c are resistances of phases a, b, and c for the equivalent circuit of a three-phase delta winding motor given in Fig. 6. $L_{ab}(=L_{ba})$, $L_{bc}(=L_{cb})$, and $L_{ca}(=L_{ac})$ are the mutual stator inductances for a–b, b–c, and c–a. Assuming the coil resistances, inductances, and mutual inductances are symmetric, $R_a = R_b = R_c = R$, $L_a = L_b = L_c = L$, and $L_{ab} = L_{bc} = L_{ca} = M$. Then, (1) can be simplified as follows.

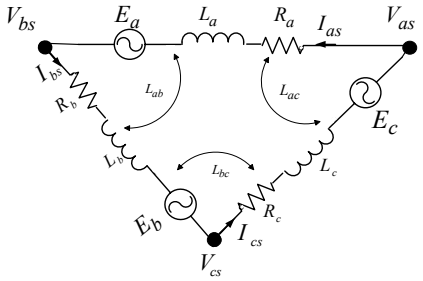

Fig. 6 Equivalent circuit of a three-phase delta-winding motor

$$\begin{bmatrix} V_{as} \\ V_{bs} \\ V_{cs} \end{bmatrix} = \begin{bmatrix} R & 0 & 0 \\ 0 & R & 0 \\ 0 & 0 & R \end{bmatrix} \begin{bmatrix} I_{as} \\ I_{bs} \\ I_{cs} \end{bmatrix} + \frac{d}{dt} \begin{bmatrix} L & M & M \\ M & L & M \\ M & M & L \end{bmatrix} \begin{bmatrix} I_{as} \\ I_{bs} \\ I_{cs} \end{bmatrix} + \begin{bmatrix} E_a \\ E_b \\ E_c \end{bmatrix} \quad (2)$$

Since $I_{as} + I_{bs} + I_{cs} = 0$, we obtain

$$MI_{bs} + MI_{cs} = -MI_{as} \quad (3)$$

Substituting (3) into (2),

$$\begin{bmatrix} V_{as}-V_{bs} \\ V_{bs}-V_{cs} \\ V_{cs}-V_{as} \end{bmatrix} = \begin{bmatrix} R & 0 & 0 \\ 0 & R & 0 \\ 0 & 0 & R \end{bmatrix} \begin{bmatrix} I_{as} \\ I_{bs} \\ I_{cs} \end{bmatrix} + \frac{d}{dt} \begin{bmatrix} L-M & 0 & 0 \\ 0 & L-M & 0 \\ 0 & 0 & L-M \end{bmatrix} \begin{bmatrix} I_{as} \\ I_{bs} \\ I_{cs} \end{bmatrix} + \begin{bmatrix} E_a \\ E_b \\ E_c \end{bmatrix} \quad (4)$$

Back-electromotive forces of phases a, b, and c can be expressed as

$$\begin{bmatrix} E_a \\ E_b \\ E_c \end{bmatrix} = \begin{bmatrix} K_e \sin(k\theta_r) \\ K_e \sin\left(k\theta_r - \frac{2\pi}{3}\right) \\ K_e \sin\left(k\theta_r - \frac{4\pi}{3}\right) \end{bmatrix} \omega_r \tag{5}$$

where K_e is the back EMF constant, ω_r is motor angular velocity, and θ_r is electrical angular displacement. Substituting (5) into (4),

$$\begin{bmatrix} V_{as}-V_{bs} \\ V_{bs}-V_{cs} \\ V_{cs}-V_{as} \end{bmatrix} = \begin{bmatrix} R & 0 & 0 \\ 0 & R & 0 \\ 0 & 0 & R \end{bmatrix} \begin{bmatrix} I_{as} \\ I_{bs} \\ I_{cs} \end{bmatrix} + \frac{d}{dt} \begin{bmatrix} L-M & 0 & 0 \\ 0 & L-M & 0 \\ 0 & 0 & L-M \end{bmatrix} \begin{bmatrix} I_{as} \\ I_{bs} \\ I_{cs} \end{bmatrix} + \begin{bmatrix} K_e \sin(k\theta_r) \\ K_e \sin\left(k\theta_r - \frac{2\pi}{3}\right) \\ K_e \sin\left(k\theta_r - \frac{4\pi}{3}\right) \end{bmatrix} \omega_r \tag{6}$$

The motor torque is expressed as

$$T_e = K_t \left[I_{as} \sin(k\theta_r) + I_{bs} \sin\left(k\theta_r - \frac{2\pi}{3}\right) + I_{cs} \sin\left(k\theta_r - \frac{4\pi}{3}\right) \right] \tag{7}$$

where K_t is the torque constant. Therefore, we have torque equation of the motor as follows.

$$T_e - T_L = J\frac{d\omega_r}{dt} + B\omega_r \tag{8}$$

where J is motor inertia; T_L is load torque; and B is damping coefficient. Therefore, based on Laplace transformation of (6), (7), and (8), we can obtain

$$\begin{bmatrix} I_{as} \\ I_{bs} \\ I_{cs} \end{bmatrix} = \begin{bmatrix} \frac{1}{(L-M)s+R} & 0 & 0 \\ 0 & \frac{1}{(L-M)s+R} & 0 \\ 0 & 0 & \frac{1}{(L-M)s+R} \end{bmatrix} \begin{bmatrix} V_{as}-V_{bs}-K_e\omega_r \sin(k\theta_r) \\ V_{bs}-V_{cs}-K_e\omega_r \sin\left(k\theta_r - \frac{2\pi}{3}\right) \\ V_{cs}-V_{as}-K_e\omega_r \sin\left(k\theta_r - \frac{4\pi}{3}\right) \end{bmatrix} \tag{9}$$

$$\omega_r = \frac{1}{Js+B}(T_e - T_L)$$

Therefore, a dynamic system block diagram of the motor with three-phase delta-winding is shown as Fig. 7.

(2) Dynamic model of motor with wye winding connection

Assuming the coil resistances, inductances, and mutual inductances are symmetric for motor with three-phase wye winding (Fig. 8), the system dynamics of the motor can be represented as follows [12]. Note that the corresponding parameters in the following are defined as sub-section 2.1.

$$\begin{bmatrix} V_{as} \\ V_{bs} \\ V_{cs} \end{bmatrix} = \begin{bmatrix} R & 0 & 0 \\ 0 & R & 0 \\ 0 & 0 & R \end{bmatrix} \begin{bmatrix} I_{as} \\ I_{bs} \\ I_{cs} \end{bmatrix} + \frac{d}{dt} \begin{bmatrix} L_a & L_{ab} & L_{ac} \\ L_{ba} & L_b & L_{bc} \\ L_{ca} & L_{cb} & L_c \end{bmatrix} \begin{bmatrix} I_{as} \\ I_{bs} \\ I_{cs} \end{bmatrix} + \begin{bmatrix} E_a \\ E_b \\ E_c \end{bmatrix} \tag{10}$$

(10) can be simplified as follows with $L_{ab} = L_{bc} = L_{ca} = M$.

$$\begin{bmatrix} V_{as} \\ V_{bs} \\ V_{cs} \end{bmatrix} = \begin{bmatrix} R & 0 & 0 \\ 0 & R & 0 \\ 0 & 0 & R \end{bmatrix} \begin{bmatrix} I_{as} \\ I_{bs} \\ I_{cs} \end{bmatrix} + \frac{d}{dt} \begin{bmatrix} L & M & M \\ M & L & M \\ M & M & L \end{bmatrix} \begin{bmatrix} I_{as} \\ I_{bs} \\ I_{cs} \end{bmatrix} + \begin{bmatrix} E_a \\ E_b \\ E_c \end{bmatrix} \tag{11}$$

Since $I_{as} + I_{bs} + I_{cs} = 0$, (11) can be rewritten as follows by (3).

$$\begin{bmatrix} V_{as} \\ V_{bs} \\ V_{cs} \end{bmatrix} = \begin{bmatrix} R & 0 & 0 \\ 0 & R & 0 \\ 0 & 0 & R \end{bmatrix} \begin{bmatrix} I_{as} \\ I_{bs} \\ I_{cs} \end{bmatrix} + \frac{d}{dt} \begin{bmatrix} L-M & 0 & 0 \\ 0 & L-M & 0 \\ 0 & 0 & L-M \end{bmatrix} \begin{bmatrix} I_{as} \\ I_{bs} \\ I_{cs} \end{bmatrix} + \begin{bmatrix} E_a \\ E_b \\ E_c \end{bmatrix} \tag{12}$$

Based on (5), (12) can be rewritten as follows.

$$\begin{bmatrix} I_{as} \\ I_{bs} \\ I_{cs} \end{bmatrix} = \begin{bmatrix} \frac{1}{(L-M)s+R} & 0 & 0 \\ 0 & \frac{1}{(L-M)s+R} & 0 \\ 0 & 0 & \frac{1}{(L-M)s+R} \end{bmatrix} \begin{bmatrix} V_{as}-K_e\omega_r \sin(k\theta_r) \\ V_{bs}-K_e\omega_r \sin\left(k\theta_r - \frac{2\pi}{3}\right) \\ V_{cs}-K_e\omega_r \sin\left(k\theta_r - \frac{4\pi}{3}\right) \end{bmatrix} \tag{13}$$

Therefore, the dynamic system block diagram of a motor with three-phase wye winding is given as shown in Fig. 9. Based on wye winding connection, a serial-wye connection is proposed, where two sets of resistors and inductors are connected in series in each phase as shown in Fig. 10. The system dynamics can be represented as follows.

$$\begin{bmatrix} I_{as} \\ I_{bs} \\ I_{cs} \end{bmatrix} = \begin{bmatrix} \frac{1}{2(L-M)s+2R} & 0 & 0 \\ 0 & \frac{1}{2(L-M)s+2R} & 0 \\ 0 & 0 & \frac{1}{2(L-M)s+2R} \end{bmatrix} \begin{bmatrix} V_{as}-K_e\omega_r \sin(k\theta_r) \\ V_{bs}-K_e\omega_r \sin\left(k\theta_r - \frac{2\pi}{3}\right) \\ V_{cs}-K_e\omega_r \sin\left(k\theta_r - \frac{4\pi}{3}\right) \end{bmatrix} \tag{14}$$

Based on a similar analysis, the system dynamics block diagram of the serial-wye connection can be shown in Fig. 11 .

Compared to wye winding of Fig. 8, the electrical impedance of the serial-wye winding as shown in Fig. 10, i.e., $2\sqrt{(L-M)^2\omega^2 + R^2}$ is two times that of the wye winding, i.e., $\sqrt{(L-M)^2\omega^2 + R^2}$, where ω is frequency. Then the torque constant K_t of the serial-wye winding is larger than that of the wye winding. For the rated output torque at a given speed, the currents in each branch of the serial-wye and wye connections remain the same. The resultant line current and line voltage, however, are different. Whereas the line current for the serial-wye connection is half of the wye connection, and the line voltage for the serial-wye connection is twice that of the wye connection under identical output conditions. A high starting torque can be achieved without over current from the inverter, if the stator windings are connected in serial-wye. Although the winding current may be twice its rated value during low-speed operation, the line current of the motor does not exceed the rated line current. During normal or high-speed operation, line voltage is limited by the battery voltage of the vehicle, in which case the wye connection is used.

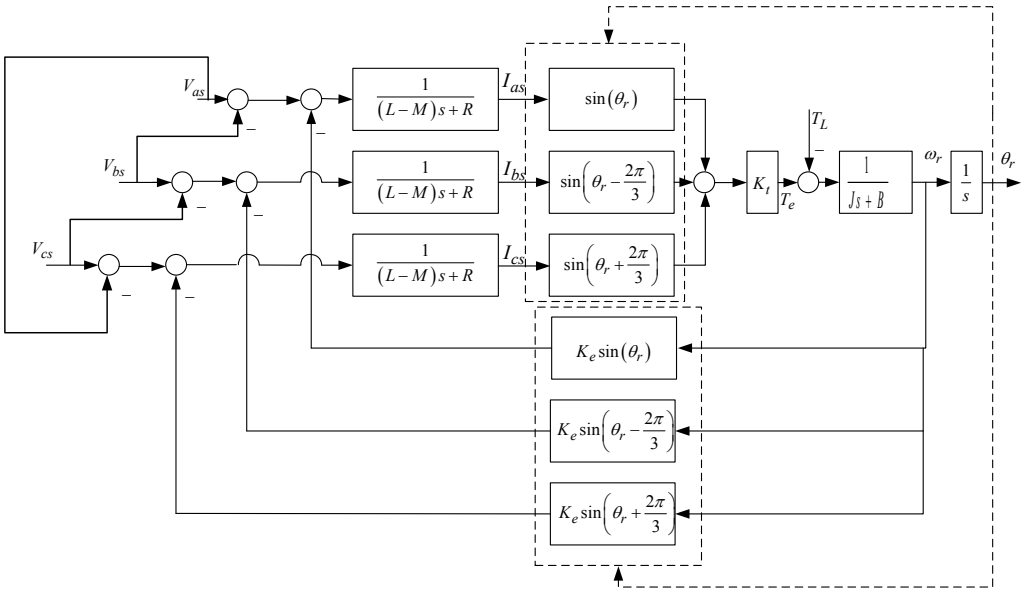

Fig. 7 Dynamic system block diagram of the motor with three-phase delta winding

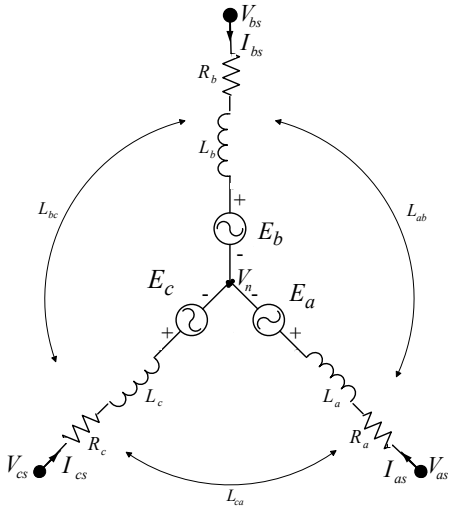

Fig. 8 Equivalent circuit of a three-phase wye-winding motor

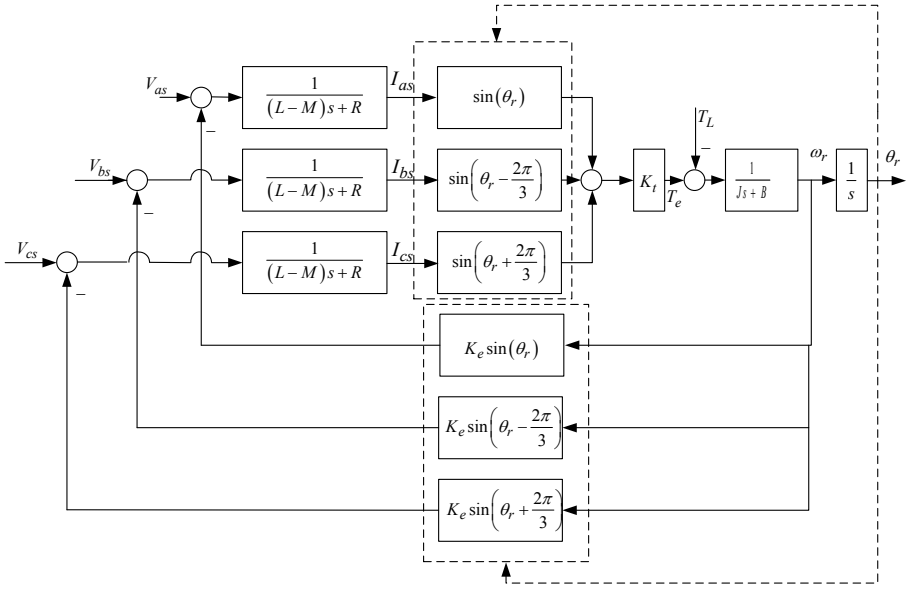

Fig. 9 Dynamic system block diagram of the motor with three-phase wye winding

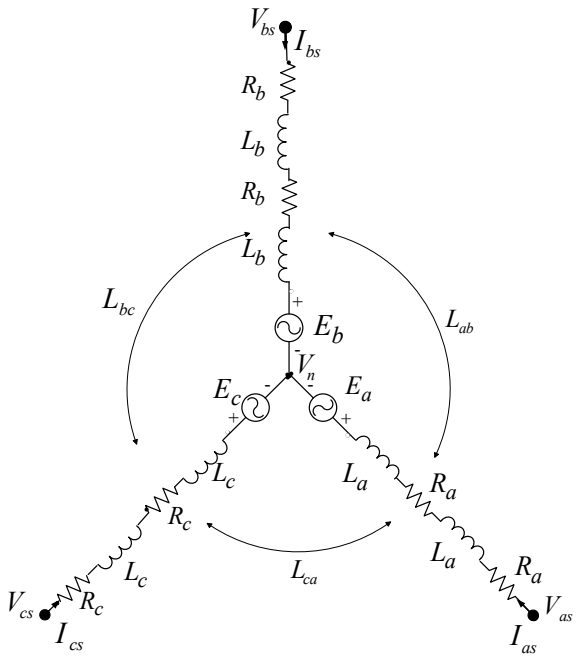

Fig. 10 Equivalent circuit of a serial-wye connection motor

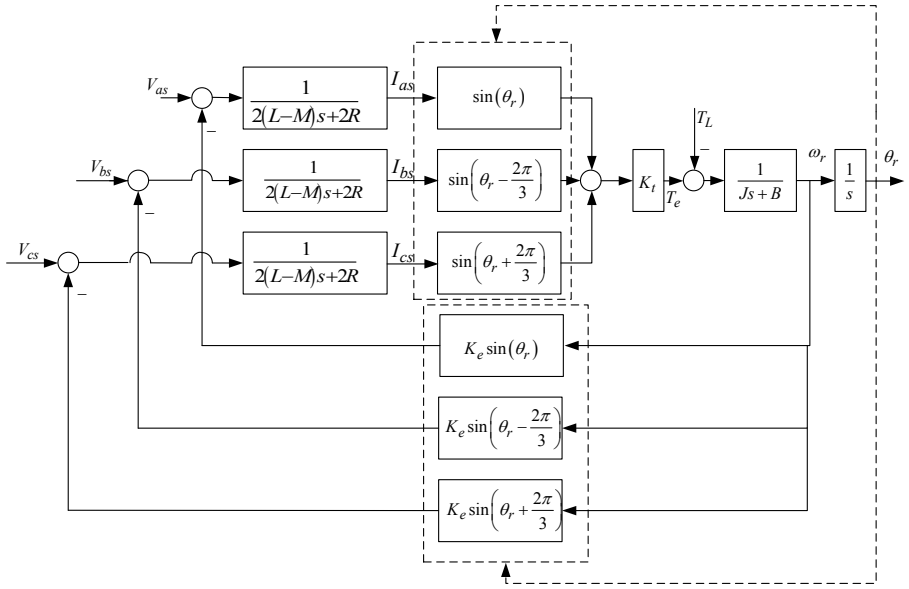

Fig. 11 Block diagram of the motor with three-phase serial-wye winding

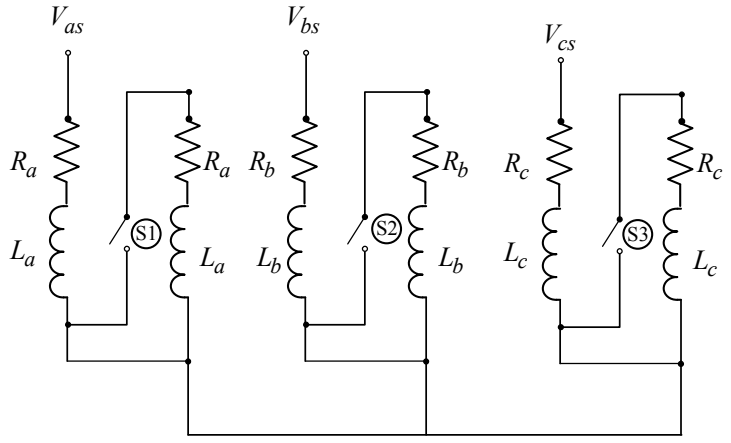

Fig. 12 Proposed dual-wye connection with three sets of switches.

The proposed dual-wye windings consist of a serial-wye and a spaced-wye connections controlled by three sets of switches as shown in Fig. 12, where the spaced-wye connection is a wye connection in this case. As motor reaching steady-state speeds, the system is switched to the wye connection mode in which S1, S2, and S3 coils are shut off, which halves the magnetic field intensity to increase the motor speed, activating the weakening control mode.

A three-phase brushless PM motor can be designed such that its stator windings comprise one set of windings as shown in Fig. 2(a). Alternatively, the stator windings can be arranged with two identical branches in parallel formation with all leads accessible outside the motor, as shown in Fig. 2 (b), which configuration is known as parallel connection. If the PM motor ratings for the Fig. 2 (a) and Fig. 2 (b) configurations are the same, no difference exists in magnetomotive force generation and terminal quantities between the two designs. In this paper, a dual-wye connection is proposed, which is connecting the motor windings in serial-wye for starting an electric vehicle and then switching the windings to spaced-wye connection for normal speed operation. With a relay or contactor, the stator winding can be readily switched from a serial-wye connection to a spaced-wye connection.

ILLUSTRATED EXAMPLE OF AFPM MOTOR DESIGN

For test purposes, a 476W AFPM motor was developed and produced in this study. The proposed AFPM motor structure in this case is illustrated by Fig. 13. The coils are formed using a mold in which the stator iron cores are subsequently inserted. The component is assembled by three-phase stator winding. The magnetic flux is generated from the interaction between the stator coil wound through the axial-flux air gap and the PM installed on the rotor back plate. Figures 14 and 15 show the winding diagram and the connections among individual coils for the motor applying the 24-slot and 16-pole configuration as an example. Each slot represents one phase, and each of the three slots represents the U, V, and W phases. Figures 14(a) and 15(a) are configured through two wye-winding cascades (U1,V1,W1 and U2,V2,W2), i.e. the serial-wye winding. This configuration features high torques required in initial drive. When the motor reaches a steady state operation, one set of wye connection (U1,V1,W1) is shut and only the other set of wye connection (U2,V2,W2), i.e. the spaced-wye winding, remains in operation as shown in Fig. 14(b) and 15(b). The corresponding magnetic field is reduced by half to result in flux weakening. Consequently, short windings reduce electrical impedance and increase current and speed.

(a) (b) (c) (d)

Fig. 13 Schematic AFPM motor assembly: (a) stator, (b) coil, (c) magnet, and (d) back plate

If the motor configuration is directly switched from serial-wye to wye connections, the coils tend to produce high surge currents. To prevent jerking and jolting at the transition between wye and serial-wye connections, a profile planning is used to design the dual duty scheme. The aim of the profile is to keep precision and speed while reducing the residual vibration. As pointed before, jerk achieves finite values for the profile, which makes the movement more fluent. In this paper, a wide range of output power regulation is provided, and a smooth planning is adopted in the winding switch. The proposed soft switch scheme is given as follows,

$$\begin{aligned}\begin{bmatrix} I_{as} \\ I_{bs} \\ I_{cs} \end{bmatrix} &= A_1 \begin{bmatrix} I_{as1} \\ I_{bs1} \\ I_{cs1} \end{bmatrix} + A_2 \begin{bmatrix} I_{as2} \\ I_{bs2} \\ I_{cs2} \end{bmatrix} \\ &= A_1 \frac{1}{2(L-M)s+2R} \begin{bmatrix} V_{as}-E_{as} \\ V_{bs}-E_{bs} \\ V_{cs}-E_{cs} \end{bmatrix} + A_2 \frac{1}{(L-M)s+R} \begin{bmatrix} V_{as}-E_{as} \\ V_{bs}-E_{bs} \\ V_{cs}-E_{cs} \end{bmatrix}\end{aligned} \tag{15}$$

where A_1 and A_2 should be selected such that $A_1 + A_2 = 1$. The switch point of the winding is assumed at certain speed ω_s and the area of the smooth switch is given as $\pm\Delta\omega$. For $\omega_r \le (\omega_s - \Delta\omega)$, as shown in Fig. 16, the motor is operated by the serial-wye winding, i.e., $A_2 = 1$ and $A_1 = 0$, while $\omega_r \ge (\omega_s + \Delta\omega)$, the motor is operated by the wye winding, i.e., $A_2 = 0$ and $A_1 = 1$. A_1 and A_2 are determined by (16) and (17) respectively.

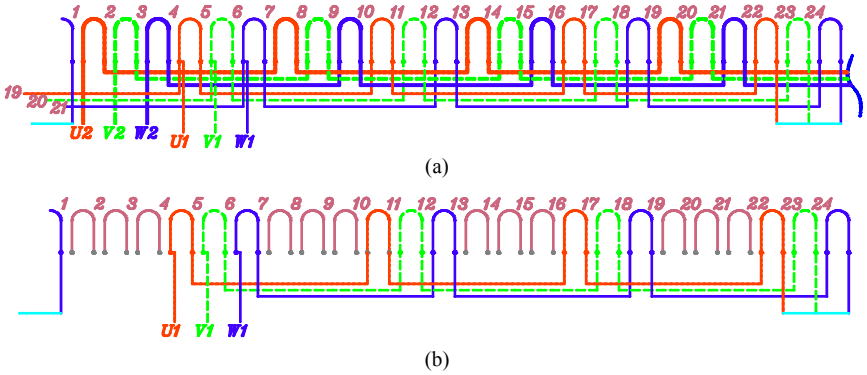

Fig. 14 Winding diagram and the connections among individual coils of the illustrated example using (a) serial-wye connection and (b) spaced-wye connection

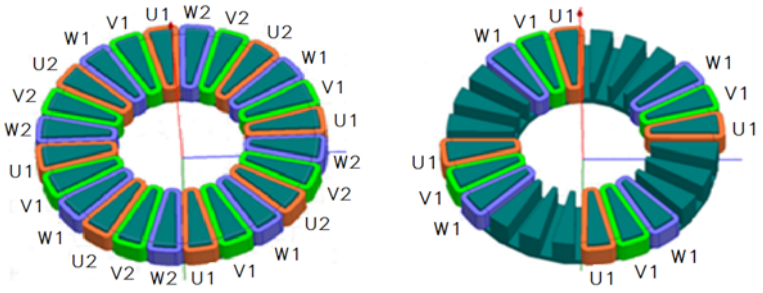

(a) (b)

Fig. 15 Schematic representations of the illustrated example:

(a) serial-wye winding stator and (b) spaced-wye winding stator

$$A_1=\begin{cases} u(\omega_s-\Delta\omega-\omega_r) & ,\forall 0\le\omega_r\le(\omega_s-\Delta\omega) \\ \frac{1}{4}\cos\left(\frac{\omega_r-(\omega_s-\Delta\omega)}{\Delta\omega}\pi\right)+\frac{3}{4} & ,\forall(\omega_s-\Delta\omega)<\omega_r<\omega_s \\ \frac{1}{4}\cos\left(\frac{\omega_r-\omega_s}{\Delta\omega}\pi\right)+\frac{1}{4} & ,\forall\omega_s\le\omega_r<(\omega_s+\Delta\omega) \\ 0 & ,\forall(\omega_s+\Delta\omega)\le\omega_r \end{cases} \quad (16)$$

$$A_2=\begin{cases} 0 & ,\forall 0\le\omega_r\le(\omega_s-\Delta\omega) \\ \frac{1}{4}-\frac{1}{4}\cos\left(\frac{\omega_r-(\omega_s-\Delta\omega)}{\Delta\omega}\pi\right) & ,\forall(\omega_s-\Delta\omega)<\omega_r<\omega_s \\ \frac{3}{4}-\frac{1}{4}\cos\left(\frac{\omega_r-\omega_s}{\Delta\omega}\pi\right) & ,\forall\omega_s\le\omega_r<(\omega_s+\Delta\omega) \\ u(\omega_s+\Delta\omega-\omega_r) & ,\forall(\omega_s+\Delta\omega)\le\omega_r \end{cases} \quad (17)$$

Where $u(x)$ is unit function for $u(x)$=1, $x\geqq 0$ and $u(x)$=0, $x<0$. An example is used to illustrate the proposed switch method, where the parameters of ω_s = 500 *rpm*, $\Delta\omega$ = 50 *rpm*, and ω_r = 0~1000 *rpm* are given and the simulated result is shown in Fig. 17. The proposed soft switch method is applied for the switch between serial-wye and spaced-wye winding connections as shown in Fig. 18.

DESIGN SIMULATION AND EXPERIMANT

Simulation of the proposed AFPM motor

The proposed AFPM motor consisted of 24 slots and 16 poles is applied to illustrate the winding design. The specifications are listed in Table 1 and the parameters for the theoretical model of voltage input to velocity output are shown in Table 2. The time responses of current and velocity of AFPM motor with serial-wye and spaced-wye winding connections are simulated by the system block diagrams in Fig. 9 and Fig. 11 respectively.

Finite element method is used to simulate 3D magnetic field intensities of serial-wye and spaced-wye windings as shown in Fig. 19. The simulations illustrate the excitation between every grouping of motor stator slots and the rotor poles. The magnetic lines of force circulate vertically between the rotor magnets and the back plate spacers. Only half the regions of the wye connections present the magnetic flux for the spaced-wye winding as shown in Fig. 19(b) indicating that the weakening effect was approximately half those of the serial-wye winding in Fig. 19(a). The phase currents of the motor are simulated with the phase voltage of 48V and the load torque of 5 Nm. The velocity of spaced-wye is 180 rad/s as shown in Fig. 20, and that of serial-wye winding are about 125 rad/s as shown in Fig. 24.

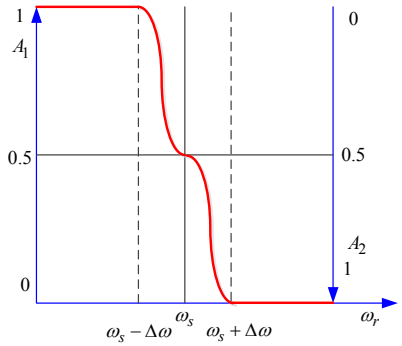

Fig. 16 Proposed soft switch scheme

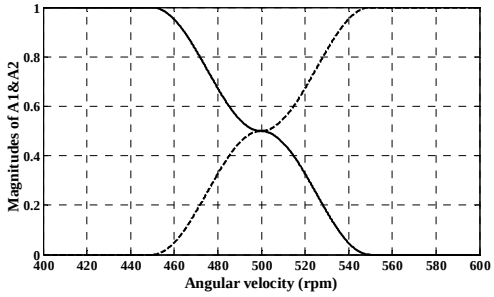

Fig. 17 Magnitudes of A_1 (solid-line) and A_2 (dashed-line) for the given example.

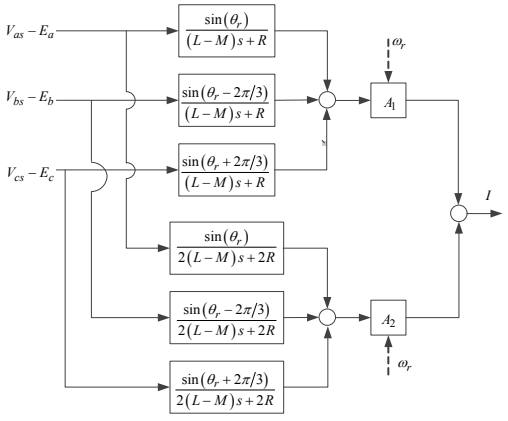

Fig. 18 Proposed soft switch method for serial-wye and wye winding connections

Table 1. AFPM motor specifications

Number of phases	Three
Rated speed/serial-wye	600 (rpm)
Input voltage	48 (V)
Number of rotor poles	16
Number of stator slots	24
Power	746 (W)
Outer stator diameter	164 (mm)
Inner stator diameter	90 (mm)
Motor thickness	40 (mm)
Air gap	3.0 (mm)

Table 2. Parameters of the simulated model

Torque constant (K_t), (Nm/A)	0.33
Back electromotive force constant (K_e), (V/rad/sec)	0.33
Winding resistance (R), (Ω)	0.71
Winding inductance (L), (mH)	1.54
Mutual inductance (M), (mH)	0.45
Rotor inertia (J), (Kg · cm^2)	5.4
Damping coefficient (B), (N-m-s/rad)	0.000561

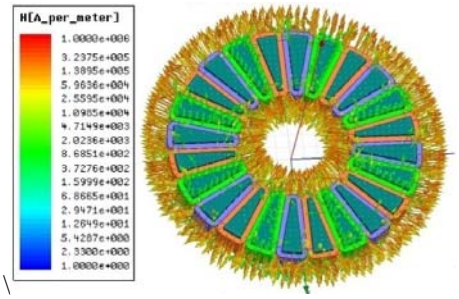

(a)

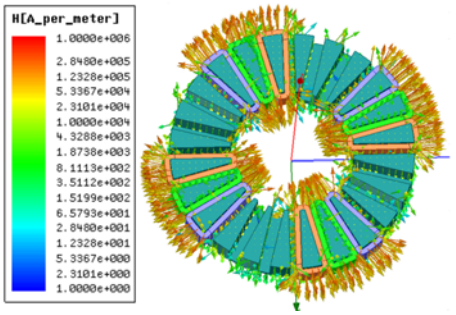

(b)

Fig. 19 FEM simulations of magnetic flux in (a) serial-wye and (b) spaced-wye configurations

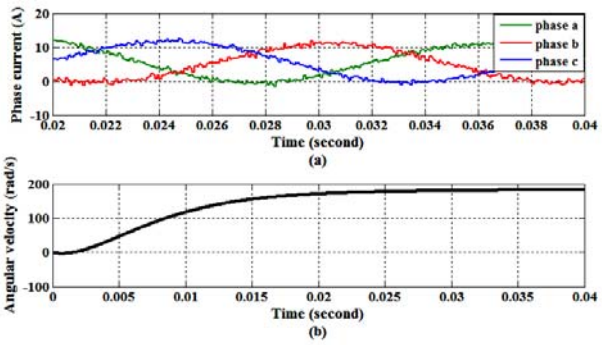

Fig. 20 Time responses of (a) phase currents and (b) angular velocity for spaced-wye winding

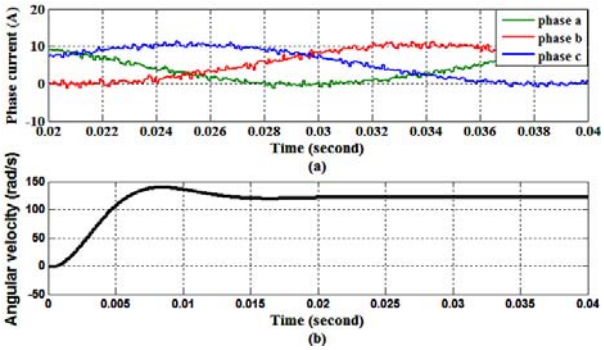

Fig. 21 Time responses of (a) phase currents and (b) motor angular velocity for serial-wye winding

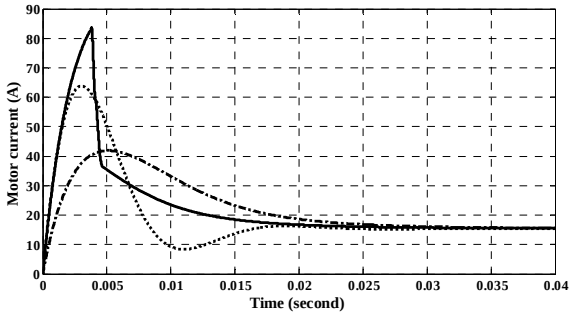

Fig. 22 Transient responses of motor current with serial-wye winding (dash-dotted line), spaced-wye winding (dotted line), and dual-wye windings and soft switch (solid line)

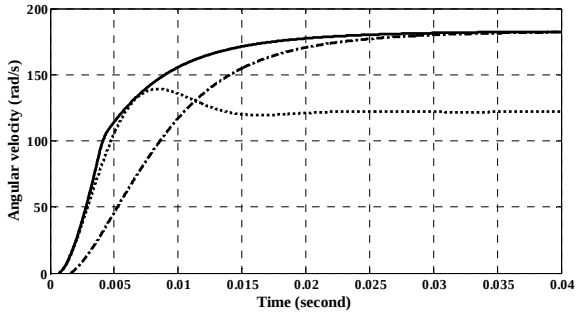

Fig. 23 Time responses of motor velocities with spaced-wye winding (dash-dotted line), serial-wye winding (dotted line), and dual-wye windings and soft switch (solid line)

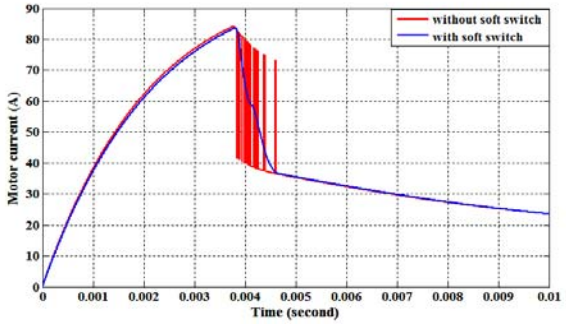

Fig. 24 Transient Responses of motor current with/without soft switch

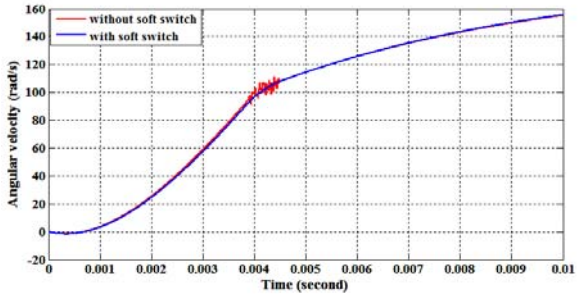

Fig. 25 Time responses of motor velocity with/without soft switch

Fig. 22 compares the transient responses of motor currents. The maximun current of serial-wye winding is about 40A, and that of spaced-wye winding is about 65A. The steady state currents of both windings are 16A. Through the proposed soft switch method of (15)-(17), the current of serial-wye winding can be smoothly transitted to that of spaced-wye winding. The related motor velocities of the serial-wye and spaced-wye windings are given in Fig. 23, where the steady state motor velocity of the spaced-wye winding is at 180 rad/s, and that of serial-wye is at 125 rad/s . By the proposed soft switch method, the steady state velocity can be smoothly adopted from 125 rad/s to 180 rad/s. Note that ω_s=100 rad/s and $\Delta\omega$=10 rad/s are assumed in the soft switch scheme. The comparisions of the currents and the velocities in Fig. 24 and Fig. 25 show incontinuity during 0.0039~0.0045 second for the connection without soft switch, which could result in a huge vibration under direct winding switch.

Experimental results

A prototype of the illustrated motor is constructed as shown in Fig. 26. A measurement platform is established as in Fig. 27 to verify the proposed dual-wye windings and soft switch method. A drive motor connected to the AFPM motor serves as a variable load measured by a torque meter. The angular position is measured by an encoder and least-squares fit is used to estimate motor velocity [12].

The circuit and switch controller of the proposed dual-wye windings is shown in Fig. 28, where three flywheel diodes are integrated into a three-phase full-bridge circuit and Hall sensors are used to detect rotor position. Three-phase voltages of the AFPM motor with 120° rectangular wave driven are gererated by 3-step pulse control IGBT switching. The switch between serial-wye and spaced-wye windings are realized by solid state relays (SSRs).

(a) (b) (c)

Fig. 26 Prototyped AFPM motor with dual-wye windings: (a) rotor, (b) stator, and (c) direct drive hub motor assembly

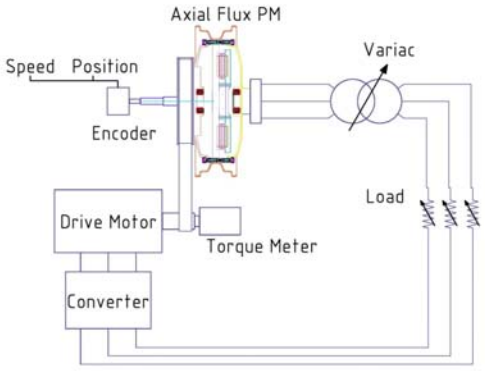

Fig. 27 Dynamic measurement platform

Figure 29 compares the torque and velocity characteristics of the proposed AFPM motor with serial-wye winding, spaced-wye winding, and dual-wye windings with soft switch. The results show that the motor velocity can be increased from 125 rad/s to 180 rad/s smooth by the proposed soft switch method. When the serial-wye connection was used at low speeds for activation, the AFPM motors can generate large torques. When reaching a steady state, the motor was switched to a spaced-wye winding, which the motor velocities can be increased.

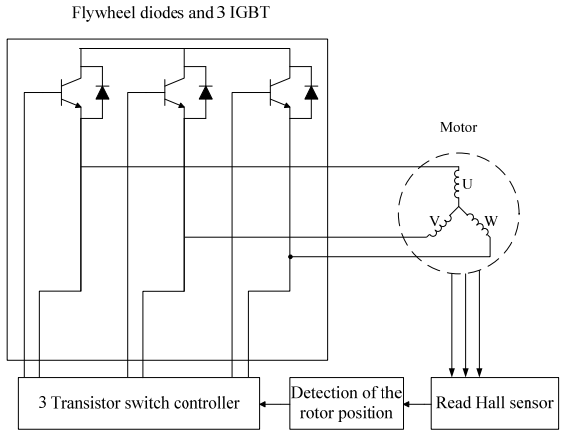

Fig. 28 Schematic of the proposed circuit and switch controller

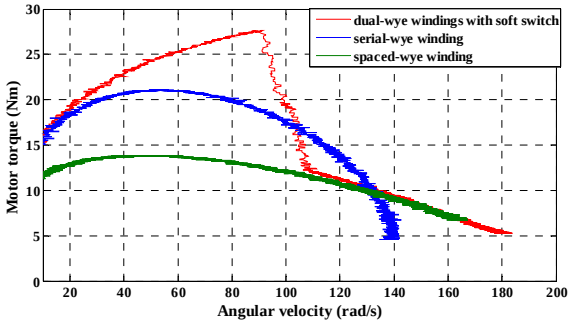

Fig. 29 Relationships of torque and velocity on serial-wye and spaced-wye windings with soft switch, spaced-wye winding, and serial-wye winding

CONCLUSION

This paper presented an alternative approach to the design of an AFPM motor with variable winding switch for in-wheel drive vehicle applications. A novel excitation winding design using a switched dual-wye connection was presented. The serial-wye winding provides high driving torque at startup and the spaced-wye winding increases motor speed at a steady state. The theoretical modeling of the AFPM motor with variable windings configuration is constructed. Moreover, the soft switch method of variable windings for reducing magnetic flux coupling was designed to prevent vibration at the switching point. A prototype AFPM motor with rated 476W output power at 125 rad/s rotation velocity has been constructed and was used to verify the proposed switch scheme. The results indicate that, by switching a serial-wye winding to a spaced-wye winding, the magnetic field is reduced by 50% and motor speed can be increased by 44% under a 5 Nm load condition.

REFERENCES

[1] Y. P. Yang, Y. P. Luh, and C. H. Cheung, "Design and control of axial-flux brushless DC wheel motors for electric Vehicles-part I: multiobjective optimal design and analysis," IEEE Transactions on Magnetics, vol. 40, no. 4, pp. 1873-1882, July 2004.

[2] Wu, L. Song and S. Cui, "Study on improving the performance of permanent magnet wheel motor for the electric vehicle application," IEEE Transactions on Magnetics, vol.43, no.1, pp.438-442, Jan. 2007.

[3] Y. P. Yang, C. H. Lee, and P. C. Hung, "Multi-objective optimal design of an axial-flux permanent-magnet wheel motor for electric scooters," IET Electric Power Applications, vol. 8, no.1, pp. 1-12, Jan. 2014.

[4] C. C. Jensen, F. Profumo, and T. A. Lipo, "A low loss permanent magnet brushless DC motor utilizing tape wound amorphous iron," IEEE Transactions on Industry Applications, vol. 28, no.3, pp.646-651, May/June 1992.

[5] A.M. EL-Refaie, "Fractional-slot concentrated-windings synchronous permanent magnet machines: Opportunities and challenges," IEEE Transaction on Industrial Electronics, vol.57, no.1, pp. 107-121, Jan. 2010.

[6] F. Caricchi, F. G. Capponi, F. Crescimbini, and L. Solero, "Experimental study on reducing cogging torque and no-load power loss in axial-flux permanent machines with slotted winding," IEEE Transactions on Industry Applications, vol. 40, no. 4, pp. 1066-1075, July. 2004.

[7] A. M. EL-Refaie, T. M. Jahns, P. J. Mc Cleer, and J. W. Mc Keever, "Experimental verification of optimal flux weakening in surface PM machines using concentrated windings," IEEE Transactions on Industry Applications, vol.42, no.2, pp. 443-453, Mar/Apr. 2006.

[8] H. Vansompel, P. Sergeant, L. Dupr´e, and A. Van den Bossche, "A combined wye-delta connection to increase the performance of axial-flux PM machines with concentrated windings," IEEE Transactions on Energy Conversion, vol. 27, no. 2, pp. 403-410, June 2012.

[9] B. J. Pleiss, "Induction motor winding," US4675591 A, Jun.1987.

[10] H. Auinger, "Circuit and winding arrangement for a multiphase electric rotating field machine," US4890049 A, Dec. 1989.

[11] T.L. Chern, J. Chang, and G. K. Chang, "DSP-Based Integral Variable Structure Model Following Control for Brushless DC Motor Drivers," IEEE Transactions on Power Electronics, vol.12, no.1, pp. 53-63, Jan. 1997.

[12] R.H. Brown, S.C. Schneider, and M.G. Mulligan, "Analysis of algorithms for velocity estimation from discrete position versus time data," IEEE Transactions on Industrial Electronics, vol.39, no.1, pp.11-19, Feb. 1992.

可變繞組之軸向永磁馬達分析及設計

余志成 鄭明得 姚武松

國立高雄第一科技大學機械與自動化系

摘 要

本文旨在探討軸向永磁馬達之設計開發，提出一創新的激磁繞組設計，作為提高轉速的功能。而典型的輪轂馬達，係以 Wye 接型式切換成 Delta 接型式的繞組來提高馬達轉速，但有產生火花的危險。本文以 Dual-Wye 的繞線方式切換成 Skipped-Wye 的繞線方式來進行集中繞線，取代變換電流角度，可降低耦合磁通量。當馬達速度達到穩態後，再切換成 Skipped-Wye 接型式，磁場強度降低一半，此時電流上升，馬達轉速就會隨之提高，等效達到弱磁控制模式及無段變速之效果，另為了在變速後不會在切換點產生瞬間極大的加速度，以雙 Duty 切換模式，以達到平滑的轉速。本方法在高速段可提升 9.2%，且無產生火花的危險，大幅提升馬達安全性。